THE JOURNAL OF PHYSICAL CHEMISTRY A
A JOURNAL OF THE AMERICAN CHEMICAL SOCIETY

pubs.acs.org/JPCA

Article

Structural Study of $[Sc_3O_4(CO_2)_n]^+$ (n = 2, 3) Complexes by Infrared Photodissociation Spectroscopy and Density Functional Calculations

Pengcheng Liu, Jia Han,* Haili Yu, Yan Chen, and Xiaoguo Zhou

Cite This: *J. Phys. Chem. A* 2024, 128, 7158−7166

Read Online

ACCESS | Metrics & More | Article Recommendations | Supporting Information

ABSTRACT: The catalytic transformation of CO_2 into valuable products has garnered wide interest owing to both economic and environmental benefits, in which the chemical fixation of CO_2 into carbonate structures represents a crucial step that occurs on the adsorbed catalyst surfaces. Transition metal oxides with acidic and basic active sites have exhibited potential in promoting the carbonation of weakly bound CO_2 molecules. Here, the interactions between CO_2 molecules and the $Sc_3O_4^+$ cation in the gas phase are investigated by using infrared photodissociation spectroscopy in conjunction with quantum chemical calculations. Both end-on and various carbonate-containing configurations, including center and bridge carbonate structures, have been theoretically identified for the CO_2-coordinated ion−molecule complexes. Based on the comparison between the experimental spectra and simulated spectra of low-lying isomers in the CO_2 antisymmetric stretching vibrational frequency region, isomers characterized by a bridge carbonate core structure are demonstrated to be the major contributors to the observed spectra. Examination of potential energy surfaces reveals lower energy barriers and simpler reaction routes for the conversion of molecularly bound CO_2 into a bridge carbonate moiety, providing reasonable explanations for their prevalence in the experiments.

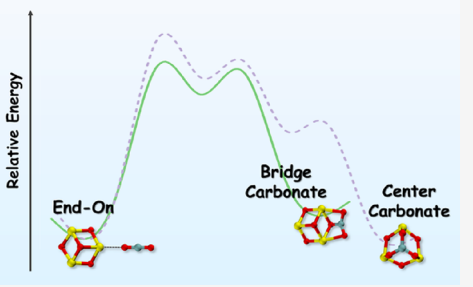

1. INTRODUCTION

The large anthropogenic CO_2 emissions into the atmosphere pose a growing threat to the global environment. Moreover, the limited availability of fossil fuels drives the search for alternative carbon sources to establish a sustainable society. Catalytic conversion of CO_2 into valuable fuels and chemicals not only offers a way to address the challenges presented by the ever-increasing energy demand but also aids in mitigating the negative impact on the environment that resulted from a fossil fuel-based economy.[1,2] In particular, the exceptional thermodynamic and kinetic stability of CO_2 makes its adsorption and activation on the active sites of catalysts a crucial stage of enormous significance.[3]

Metal oxides with both acidic and basic active sites, especially transition-metal-based oxides, have been extensively explored as highly stable and efficient adsorbents and catalysts in the transformation of CO_2.[4−6] The interactions between metal oxides and CO_2 molecules are therefore of great interest and importance in gaining insights into the associated catalytic mechanisms. State-of-the-art spectroscopic and theoretical methods have been utilized to explore the nature of the CO_2 adsorption products on metal oxide surfaces, with infrared spectroscopy being a widely employed technique in this in situ research.[7,8] However, because of the complexity of surface structure and the presence of coadsorbates, the exact binding modes and associated mechanisms of CO_2 adsorption on metal oxides are still under debate. Different species, including linear and bent CO_2, monodentate and polydentate carbonate, as well as carboxylate species, have been identified upon CO_2 adsorption on the surface of various metal oxides.[9,10]

The matrix isolation spectroscopic technique has been predominantly employed to investigate the thermodynamics and mechanisms of reactions between neutral metal oxides and CO_2 molecules by trapping and identifying the reactive intermediates.[11] For instance, researchers studied the reaction products of NbO and NbO_2 molecules with CO_2 using matrix isolation infrared spectroscopy.[12] It was reported that the NbO molecule is able to spontaneously reduce CO_2 to form the carbonyl complex $NbO_2(\eta^1-CO)$ on annealing in solid neon, whereas the NbO_2 molecule reacts with CO_2 to form complexes with three different coordination modes. The interactions of TiO and TiO_2 molecules with CO_2 have also been studied using a similar method, in which the insertion reaction of TiO molecule into the C═O bond of CO_2 under visible light excitation was confirmed, as well as the formation of an $OTiCO_3$ complex upon CO_2 attachment to TiO_2 molecule.[13] The oxo-carbonate complex has also been

Received: June 22, 2024
Revised: July 31, 2024
Accepted: August 13, 2024
Published: August 17, 2024

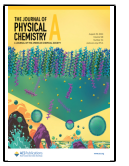

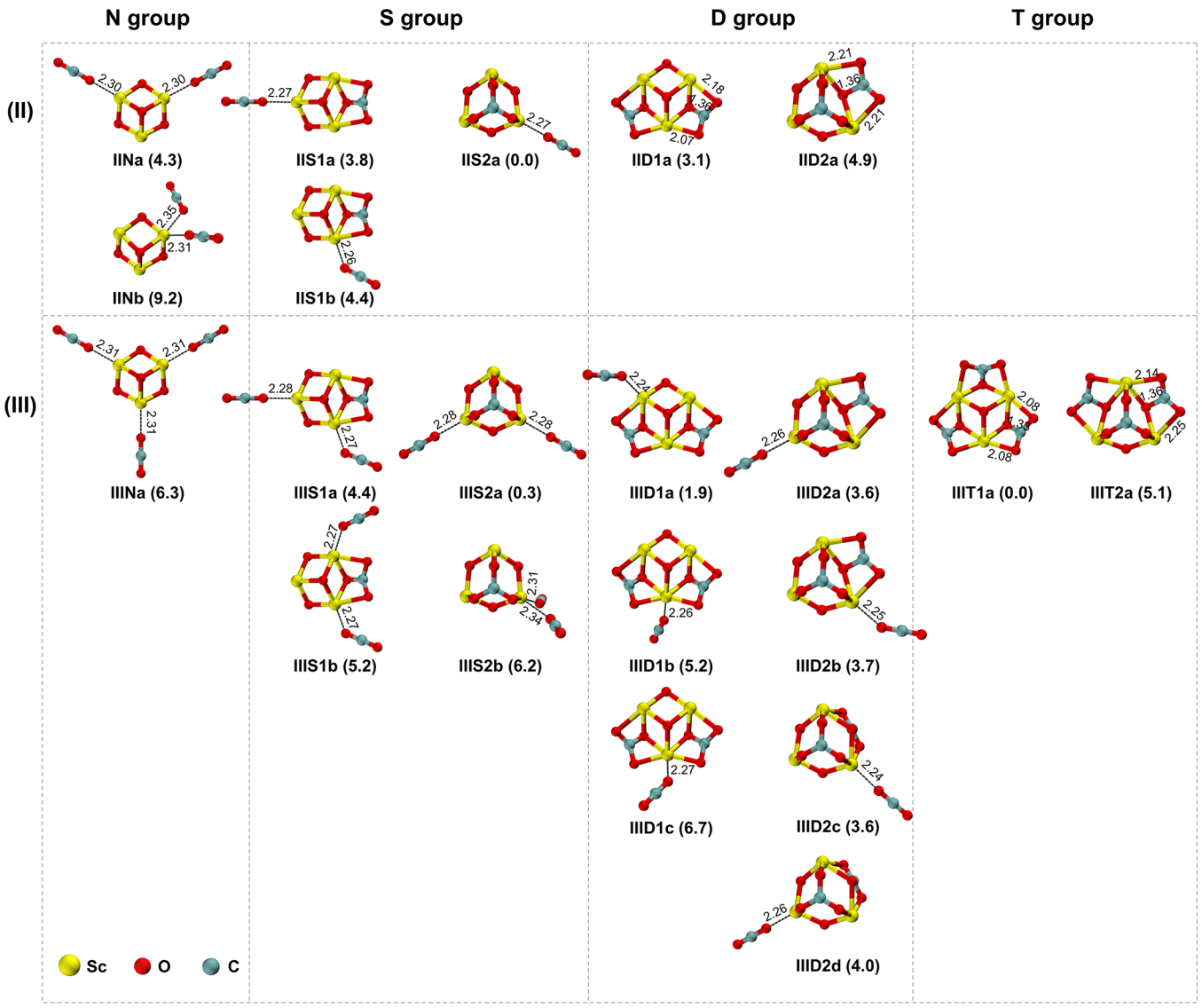

Figure 1. Low-lying structures of $[Sc_3O_4(CO_2)_n]^+$ (n = 2−3) ion−molecule complexes calculated at the PBE0-D3(BJ)/def2-TZVP level of theory. The numbers within parentheses denote the relative Gibbs free energies at 298 K (in kcal mol^{-1}). Bond lengths are noted in Å.

observed in the reactions between the ground-state ScO molecule and CO_2 on annealing.[14]

More recently, the gas-phase study of CO_2 molecules with metal oxides as model adsorbents/catalysts has become an effective approach to obtaining molecular-level details of the surface chemistry at the metal oxide−CO_2 interface, as well as to exploring the potential impacts of metals, oxidation states, and charge states on the adsorption and activation processes. Mass spectrometric analysis in tandem with laser spectroscopy has proven to be a powerful method for characterizing the structure of key species in the reactions of CO_2 with charged metal oxides. Previous studies have determined the activation of CO_2 to CO and the production of oxocarbonyl complex through oxygen atom transfer reactions when a CO_2 molecule attaches to NbO^+, HfO^+, TaO^+, and WO^+ monoxide cations.[15,16] Upon further coordination of CO_2 ligands, scandium oxides, including ScO^+ and $Sc_2O_2^+$, along with YO^+ and HoO^+ cations have shown the capability to facilitate CO_2 fixation into carbonate groups.[17−20] In contrast, there has been significantly less research on the reactivity of highly oxygenated metal oxide cations toward the carbonation of CO_2 molecules. No significant CO_2 activation has been observed in the reactions of NiO_2^+, NbO_2^+, TaO_2^+, and TaO_3^+ cations with multiple CO_2 molecules.[21−24]

In the present study, the interaction between the $Sc_3O_4^+$ cation and CO_2 molecules in the gas phase is investigated by the combination of infrared photodissociation spectroscopy and density functional theory (DFT) calculations as a step toward a better understanding of the activity of scandium oxides with regard to CO_2 adsorption and carbonation. Theoretical explorations reveal the coordination of CO_2 in an end-on fashion, as well as bridge and center carbonate structures in $[Sc_3O_4(CO_2)_n]^+$ cationic complexes. Subsequent analyses of the recorded infrared photodissociation spectra, along with potential energy surface studies, suggest the favored formation of bridge carbonate structures under the current experimental conditions, providing mechanistic insights into the adsorption and carbonation of CO_2 molecules by scandium oxide cations.

https://doi.org/10.1021/acs.jpca.4c04163
J. Phys. Chem. A 2024, 128, 7158−7166

2. METHODS

2.1. Experimental Methods. The cationic ion−molecule complexes were generated using a laser vaporization ion source and were subjected to infrared photodissociation as described previously.[19] Briefly, a 532 nm laser (second harmonic of an Nd:YAG laser, Beamtech, Dawa-100) was employed to vaporize a scandium disk target in both translational and rotational motion. The cationic complexes were produced by the reactions of the vaporized species with CO_2 molecules in the presence of a He carrier gas seeded with 10% CO_2 (Figure S1). Backing pressure of the reaction gas was adjusted in the range of 4.0−6.0 × 10^5 Pa to obtain desired ion intensities and size distributions. After free expansion, the ions of interest were skimmed, mass-selected, and decelerated into the extraction region of a second-stage time-of-flight (TOF) mass spectrometer and then intersected by a tunable IR laser. The fragment ions and the undissociated parent ions were both reaccelerated and collected by a second-stage TOF mass spectrometer. The tunable IR laser was generated by a tabletop optical parametric oscillator/amplification (OPO/A) laser system (Laser Vision) pumped by an Nd:YAG laser (Continuum, Surelite EX). Typical infrared photodissociation spectra were recorded by monitoring the relative yield of fragment ions as a function of IR photon energy and were normalized to the IR laser energy. Tunable IR radiation was scanned in steps of 2 cm^{-1} while narrowing down to 1 cm^{-1} from 2250 to 2450 cm^{-1} for extracting detailed spectral substructures.

2.2. Theoretical Methods. Quantum chemical calculations were performed to determine the energetically low-lying structures of the target cationic complexes. Initial guess structures of the studied species were extensively generated by Genmer.[25,26] The semiempirical quantum mechanical method GFN2-xTB[27] was employed to preoptimize complex geometries using the xtb[28] program. The resulting low-energy isomers were reoptimized at the PBE0-D3(BJ)/def2-TZVP level of theory.[29,30] Vibrational frequency analyses at the same density functional level were performed to ensure that all found minima have zero imaginary frequencies, and transition states exhibit only one imaginary frequency. Intrinsic reaction coordinate (IRC) calculations were carried out to confirm that each reported transition state appropriately links the corresponding reactant and product.[31−34] All the DFT calculations were conducted with the Gaussian 16 software package.[35] The calculated harmonic vibrational frequencies were scaled by a factor of 0.957, which was determined by comparing the experimental and calculated values of the free CO_2 antisymmetric stretching vibrational frequency. Simulated IR spectra were then derived by convoluting the line spectra with Lorentzian functions with a full width at half-maximum (fwhm) of 8 cm^{-1} to reproduce spectral features.

3. RESULTS AND DISCUSSION

The $[Sc_3O_4(CO_2)_n]^+$ cationic complexes were produced by the pulsed laser vaporization of a scandium metal target in the expansion of He seeded with CO_2. The most intensive signal in the mass spectrum corresponds to the $Sc_3O_4^+$ cation, with its most stable isomer exhibiting a cage-like structure characterized by C_{3v} symmetry, as discussed in the previous study.[36] In the subsequent computational search for potential candidates for $[Sc_3O_4(CO_2)_n]^+$ ion complexes, we treated this bare ion structure as a starting point. Figure 1 shows the energetically low-lying structures found for the $Sc_3O_4^+$ core cation complexed with two or three CO_2 molecules. The relative Gibbs free energies of different isomers with respect to the corresponding global minima are also listed in Figure 1. Similar to the findings in the previous report on $[Sc_2O_2(CO_2)_n]^+$ complexes,[19] both end-on and carbonate-containing configurations were identified for each cluster size. These stable structures are classified into four subgroups, N, S, D and T, based on the amount of carbonate moieties adhering to the core structure, representing no, single, double, and triple carbonates in the complex structures, respectively. Moreover, there are two different binding motifs regarding the chemisorbed tridentate carbonate moiety, namely, the bridge carbonate where the carbon atom of CO_2 binds to a bridging oxygen of the $Sc_3O_4^+$ cation (grouped as 1) and the center carbonate binding in the center of the core structure (grouped as 2). Structures within the same subgroup that share similar binding motifs are further ordered by relative energies from low to high and are labeled as a, b, c, etc.

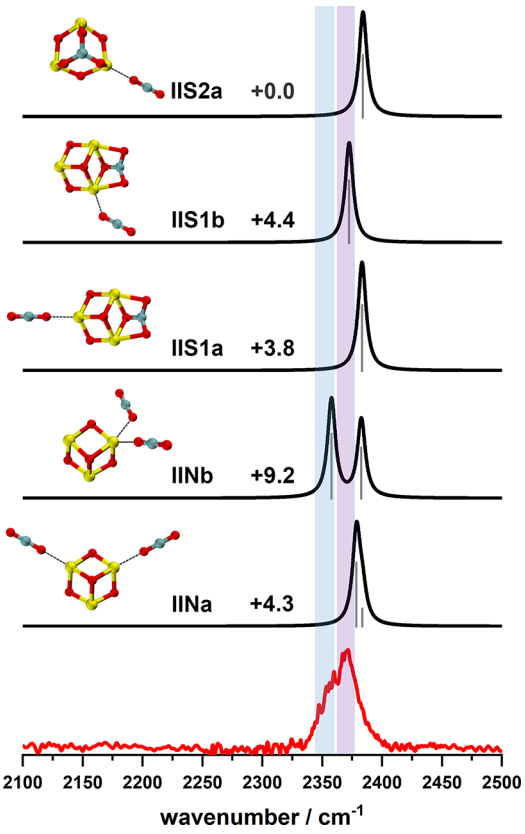

Figure 2. Experimental IRPD spectrum of the $[Sc_3O_4(CO_2)_2]^+$ ion−molecule complex in the spectral range of 2100−2500 cm^{-1} together with the simulated IR spectra of five isomers (**IINa−b**, **IIS1a−b**, and **IIS2a**) obtained at the PBE0-D3(BJ)/def2-TZVP level of theory. Relative Gibbs free energies (298 K) are given in kcal mol^{-1}.

3.1. Structure and IRPD spectrum of the $[Sc_3O_4(CO_2)_2]^+$ Ion−Molecule Complex. Figure 2 shows the experimental IRPD spectrum of the $[Sc_3O_4(CO_2)_2]^+$ ion−molecule complex complemented by the simulated IR spectra of five isomers (**IINa−b**, **IIS1a−b**, and **IIS2a**). The broad spectral band spanning from 2325 to 2407 cm^{-1} displays a prominent peak at 2371 cm^{-1} accompanied by a less intense peak at around 2359 cm^{-1} that can be resolved to some extent. The doublet spectral feature suggests the complexation of two

https://doi.org/10.1021/acs.jpca.4c04163
J. Phys. Chem. A 2024, 128, 7158−7166

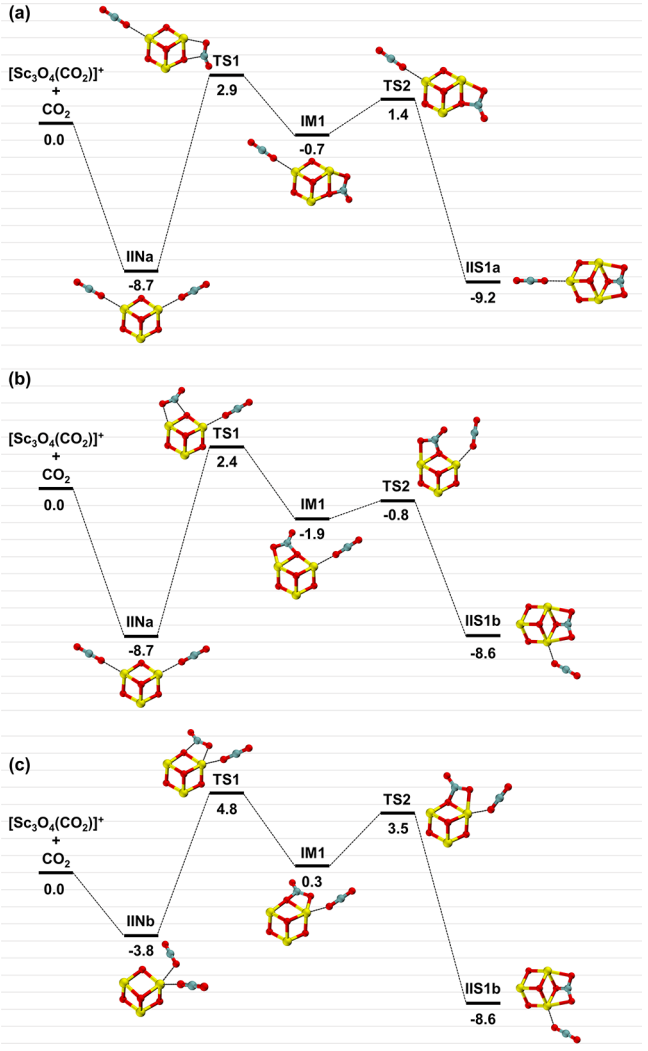

Figure 3. Reaction pathways for the transformation from isomer **IINa** to **IIS1a** (a) and **IIS1b** (b) and isomer **IINb** to **IIS1b** (c) calculated at the PBE0-D3(BJ)/def2-TZVP level of theory. Relative Gibbs free energies at 298 K are given in kcal mol^{-1}.

CO_2 molecules in different end-on binding situations or the coexistence of multiple isomers under experimental conditions. Starting from the N configuration, two low-lying isomers labeled as **IINa** and **IINb** were identified for the $n = 2$ complex, with an energy difference of 4.9 kcal mol^{-1}. Isomer **IINa** with C_s symmetry is characteristic of two CO_2 molecules molecularly bound to two equivalent Sc atoms. The vibrational frequency of the out-of-phase combination of antisymmetric stretching motions of two CO_2 molecules in isomer **IINa** is predicted to be 2379 cm^{-1}, with a markedly weaker absorption at 2384 cm^{-1} corresponding to the in-phase antisymmetric stretching combination, which yields a prominent band centered at 2379 cm^{-1}. In isomer **IINb**, two CO_2 molecules adsorbed on the same Sc atom differ in their binding orientations and distances (two Sc···OCO distances of 2.31 and 2.35 Å), giving rise to two well-separated vibrational peaks at 2358 and 2383 cm^{-1}. For the S configuration with the bridge-carbonate core structure, the CO_2 molecule is predicted to be located at the para- or ortho-position with respect to the carbonate moiety, with an energy difference of 0.6 kcal mol^{-1}. The coordination of CO_2 at the para-site in isomer **IIS1a** with an Sc···OCO distance of 2.27 Å gives a vibrational band at 2383 cm^{-1} associated with the CO_2 antisymmetric stretch, whereas the CO_2 attachment to the ortho-site (isomer **IIS1b**) with a similar Sc···OCO distance results in a less blue-shifted CO_2 antisymmetric stretch at 2372 cm^{-1}. The center-carbonate core structure offers a single site for CO_2 adsorption, which is designated as **IIS2a** and is determined to be the most stable isomer. The frequency of the antisymmetric stretching vibration of the CO_2 molecule in isomer **IIS2a** is calculated to be 2384 cm^{-1}, blue-shifted by 13 cm^{-1} to the experimental peak. In addition, two D-group isomers with double-carbonate structural motif were located, with isomer **IID1a** featuring two symmetrical bridge carbonates and **IID2a** having one bridge and one center carbonate. Both isomers lack IR signatures in the experimentally relevant frequency ranges.

Based on the comparison between the simulated IR spectra and the observed spectrum shown in Figure 2, the vibrational frequency of the CO_2 antisymmetric stretch in isomer **IIS1b** aligns with the prominent peak at 2371 cm^{-1} in the experimental spectrum, indicating its significant contribution to the spectral signals. Moreover, the experimental peak at 2359 cm^{-1} can be reproduced by the antisymmetric stretching vibration of the weakly bound CO_2 molecule in isomer **IINb**, implying a high possibility of the presence of multiple isomeric configurations. Despite the significantly higher energy of isomer **IINb**, a more substantial dissociation yield can be expected due to the reduced number of photons required for dissociating the loosely attached CO_2 molecule (Table S1), thereby contributing to the lower-energy side of the observed IR spectrum. For the remaining three isomers (**IINa**, **IIS1a**, and **IIS2a**), the absence of clear spectral evidence does not rule out the possibility of their existence, considering their lower energy compared to that of isomer IINb on the potential energy profiles and the overlap between their absorption features and the high-energy region of experimental observations.

The formation of the most probable candidate **IIS1b** involves two main reaction pathways, including the addition of a CO_2 molecule to the $[Sc_3O_4(CO_2)]^+$ core structure featuring a bridge carbonate[36] and the conversion of N isomers with two linearly bound CO_2 molecules to structures with S configuration. In the first landscape, two of the three binding sites in the $[Sc_3O_4(CO_2)]^+$ core structure allow the generation of isomer **IIS1b** (ortho-position), whereas the remaining site is associated with isomer **IIS1a** (para-position). In the latter case, possible conversion routes starting from isomers **IINa** and **IINb** are illustrated in Figure 3. As shown in the top and middle panels, there are two plausible reaction pathways for the transformation of isomer **IINa** to S structures. Both pathways involve typical two-step processes where CO_2 activation proceeds via the formation of a bidentate carbonate intermediate structure by surmounting a substantial energy barrier associated with CO_2 distortion, ultimately resulting in a tridentate carbonate group.[19] The difference in the relative orientations of the "carbonating" CO_2 molecule with respect to the other, which remains nearly unchanged, leads to the formation of two different "S1" structures. Notably, the energy barrier heights along the potential energy curve calculated for the conversion of isomer **IINa** to **IIS1b** are lower than those calculated for the conversion to **IIS1a**, i.e., 0.5 kcal mol^{-1} lower for the first step and 1.0 kcal mol^{-1} lower for the second step. Isomer **IINb**, on the other hand, is restricted to forming isomer **IIS1b** due to the shared coordination site for two CO_2 molecules. Based on all the analyses supporting the formation

https://doi.org/10.1021/acs.jpca.4c04163
J. Phys. Chem. A 2024, 128, 7158−7166

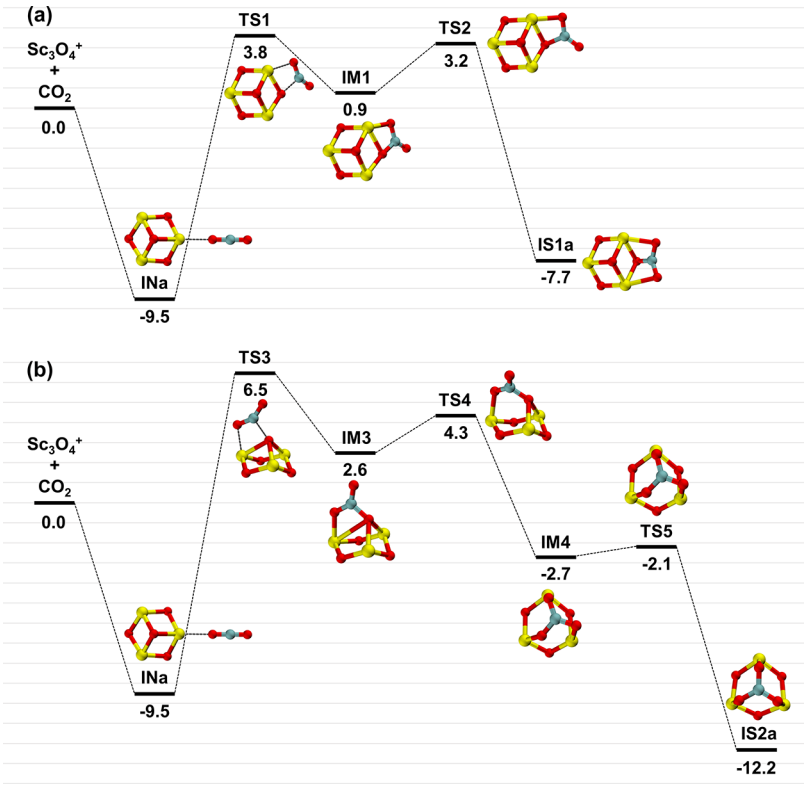

Figure 4. Reaction pathways for the transformation from the end-on isomer **INa** to the bridge-carbonate core ion **IS1a** (a) and center-carbonate core ion **IS2a** (b) calculated at the PBE0-D3(BJ)/def2-TZVP level of theory. Relative Gibbs free energies at 298 K are given in kcal mol^{-1}.

of isomer **IIS1b**, it is reasonable to consider isomer **IIS1b** as one of the dominant contributors in the experiment.

In a previous experimental and theoretical study of $[Ti_3O_6(CO_2)_n]^-$ (n = 1, 2) anion complexes,[37,38] the coexistence of a tridentate center carbonate structure as the most stable isomer and a bidentate bridge carbonate structure lying ca. 4.6 kcal mol^{-1} above the center one for n = 1 species was identified. For n = 2, the structure consisting of two carbonate moieties in the form of a bidentate bridge and a tridentate center carbonate was determined to be the major contributor. The reasons that we did not probe the spectral evidence of center carbonate structures in the present study, despite their energetic preference, are manifold. In the first place, positively charged metal oxide ions generally exhibit distinct behaviors in terms of binding patterns with CO_2 molecules compared to negatively charged species. Second, the reaction pathway for the transformation from the molecular adduct to the tridentate center carbonate structure might be more complex than that for generating the bridge carbonate structure. To validate our assumption, we conducted calculations on the reaction pathways leading from the end-on isomer to the core structures with different carbonate groups.

As illustrated in Figure 4, we have identified plausible transition states as well as intermediate structures connecting the molecularly bound form (labeled as **INa**) to different carbonate core structures (labeled as **IS1a** and **IS2a**). In the top panel, the CO_2 molecule attached to an Sc atom in **INa** first rotates around the metal atom and bends to form the TS1 structure with an energy barrier of 13.3 kcal mol^{-1}. The intermediate structure IM1, featuring a newly formed C−O bond between the bridging O atom of the $Sc_3O_4^+$ cation and the C atom of CO_2, is then accessed by passing over TS1 along the reaction coordinates. A second transition state TS2 involving the C−O bending vibration of the bidentate bound CO_2 part is required to be overcome to produce bridge carbonate core structure **IS1a**, which is associated with a considerably lower energy barrier of 2.3 kcal mol^{-1}. This two-step conversion process is nearly identical to the transformation from noncarbonate to carbonate-containing isomers of $[Sc_2O_2(CO_2)_n]^+$ complexes as described previously.[19] Alternatively, the CO_2 molecule in the end-on isomer **INa** rotates to locate on top of the $Sc_3O_4^+$ core structure to form TS3, as depicted in the bottom panel of Figure 4. The energy barrier height for this step is determined to be 16.0 kcal mol^{-1}, which is 2.7 kcal mol^{-1} higher than the energy barrier in the first stage of **IS1a** formation. In intermediate IM3, the formation of the C−O bond between the central O atom of the $Sc_3O_4^+$ cation and the C atom of CO_2 results in a bidentate carbonate moiety perpendicular to the plane defined by the three Sc atoms. By subsequent crossing of transition state TS4 with a low barrier of 1.7 kcal mol^{-1}, the perpendicularly arranged carbonate moiety overturns to form the third Sc−O bond in intermediate IM4. The resulting top carbonate parallel to the Sc plane twists over the submerged transition state TS5, eventually leading to the generation of the center carbonate core structure **IS2a**. In consideration of larger complexes, the transformation process from the end-on isomer **IINa** to the center carbonate structure **IIS2a** was investigated as illustrated in Figure S2, demonstrating a similar three-step conversion route with a higher energy barrier compared to the pathways leading to bridge carbonate isomers **IIS1a** and **IIS1b**, by 2.4 and 2.9 kcal mol^{-1}, respectively. Accordingly, the conversion of the molecular adducts to the tridentate center carbonate structures is likely to encounter higher energy barriers and substantially more intricate reaction pathways, which could

https://doi.org/10.1021/acs.jpca.4c04163
J. Phys. Chem. A 2024, 128, 7158−7166

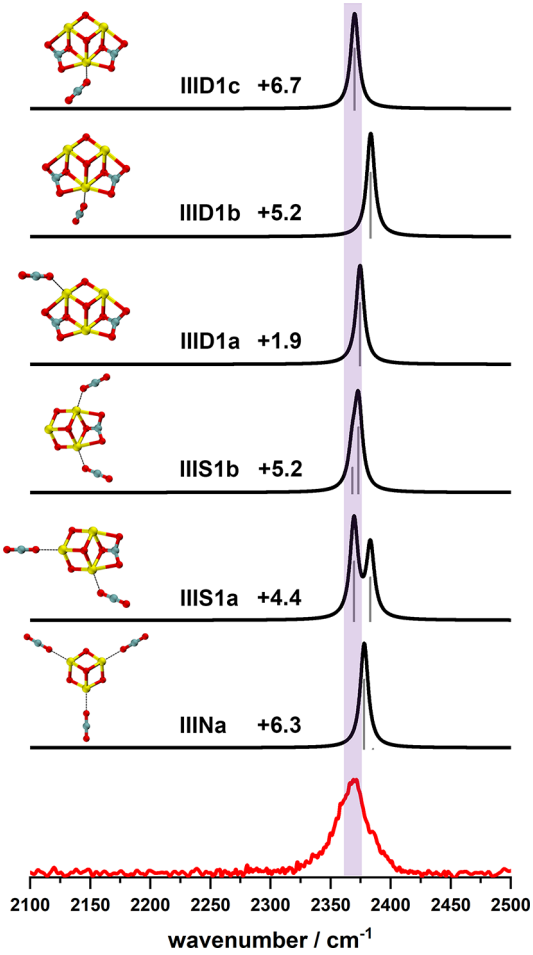

Figure 5. Experimental IRPD spectrum of the $[Sc_3O_4(CO_2)_3]^+$ ion–molecule complex in the spectral range of 2100–2500 cm^{-1} together with the simulated IR spectra of six isomers (**IIINa**, **IIIS1a–b**, and **IIID1a–c**) obtained at the PBE0-D3(BJ)/def2-TZVP level of theory. Relative Gibbs free energies (298 K) are given in kcal mol^{-1}.

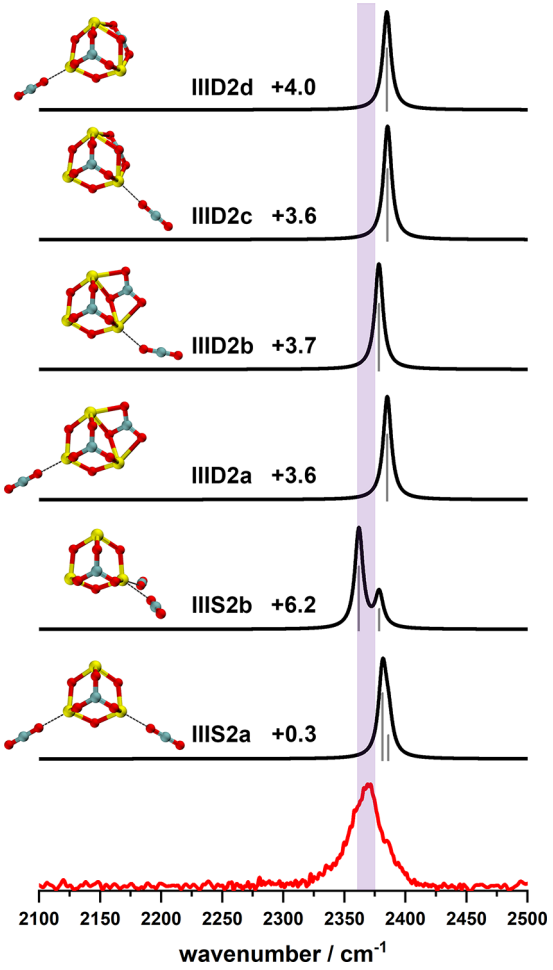

Figure 6. Experimental IRPD spectrum of the $[Sc_3O_4(CO_2)_3]^+$ ion–molecule complex in the spectral range of 2100–2500 cm^{-1} together with the simulated IR spectra of six isomers (**IIIS2a–b** and **IIID2a–d**) obtained at the PBE0-D3(BJ)/def2-TZVP level of theory. Relative Gibbs free energies (298 K) are given in kcal mol^{-1}.

hinder the formation of energetically low-lying complexes with a center carbonate structural motif.

3.2. Structure and IRPD Spectrum of the $[Sc_3O_4(CO_2)_3]^+$ Ion–Molecule Complex. For complexes with three CO_2 molecules, the experimental spectrum (red curve in Figure 5) exhibits a broad feature ranging from 2322 to 2410 cm^{-1} with a maximum at 2369 cm^{-1}. Simulated IR spectra of six representative low-lying isomers from N, S1, and D1 groups are also displayed in Figure 5. For the N structural motif, the low-lying isomer **IIINa** with C_{3v} symmetry consists of the $Sc_3O_4^+$ core ion with three CO_2 molecules bound to three equivalent Sc atoms via charge-quadrupole interactions. Due to its symmetric geometry, **IIINa** is characteristic of coupled CO_2 oscillators, including the out-of-phase combination of antisymmetric stretching modes of three equivalent CO_2 ligands and the out-of-phase combination of antisymmetric stretching vibrations of two CO_2 molecules. Both IR absorptions are predicted to be at 2378 cm^{-1}, producing a prominent peak after broadening. Among the S1 category, isomers **IIIS1a** and **IIIS1b** can be viewed as **IIS1b** solvated by an additional CO_2 molecule. Isomer **IIIS1a** shows a strong peak at 2370 cm^{-1} associated with the CO_2 molecule at the para-site, along with a relatively weak peak at 2383 cm^{-1} attributed to the CO_2 molecule at the ortho-site. In the isomer **IIIS1b** with C_s symmetry where both CO_2 ligands coordinate to the para-sites, the out-of-phase and in-phase combinations of CO_2 antisymmetric stretching modes are predicted to be at 2368 and 2373 cm^{-1}, respectively. These frequencies are too close to be discerned, yielding a prominent band centered at 2372 cm^{-1}. For the D1 group with a double-bridge carbonate core structure, the addition of a third CO_2 molecule results in a single peak in the CO_2 antisymmetric stretching region. The CO_2 antisymmetric stretching vibrational frequencies of isomers **IIID1a–c** are calculated to be at 2374, 2383, and 2370 cm^{-1}, respectively. It should be noted that the spectral band in the 2330–2400 cm^{-1} range is actually of limited use in distinguishing between isomeric structures, especially for larger complexes. This is because there are usually multiple isomers close in energy coexisting in experiments, and all probed isomeric forms contain one or more CO_2 molecules terminally bound to metal atoms. The overlapping of numerous absorptions causes congestion in the experimental spectra, making it challenging to clearly conduct the vibrational assignment. In this work, we tentatively attribute the observed peak at 2369 cm^{-1} to the major contributions of isomers **IIIS1a** and **IIID1c**, with the potential existence of other conformers shown in Figure 5 in the ion beam.

https://doi.org/10.1021/acs.jpca.4c04163
J. Phys. Chem. A 2024, 128, 7158–7166

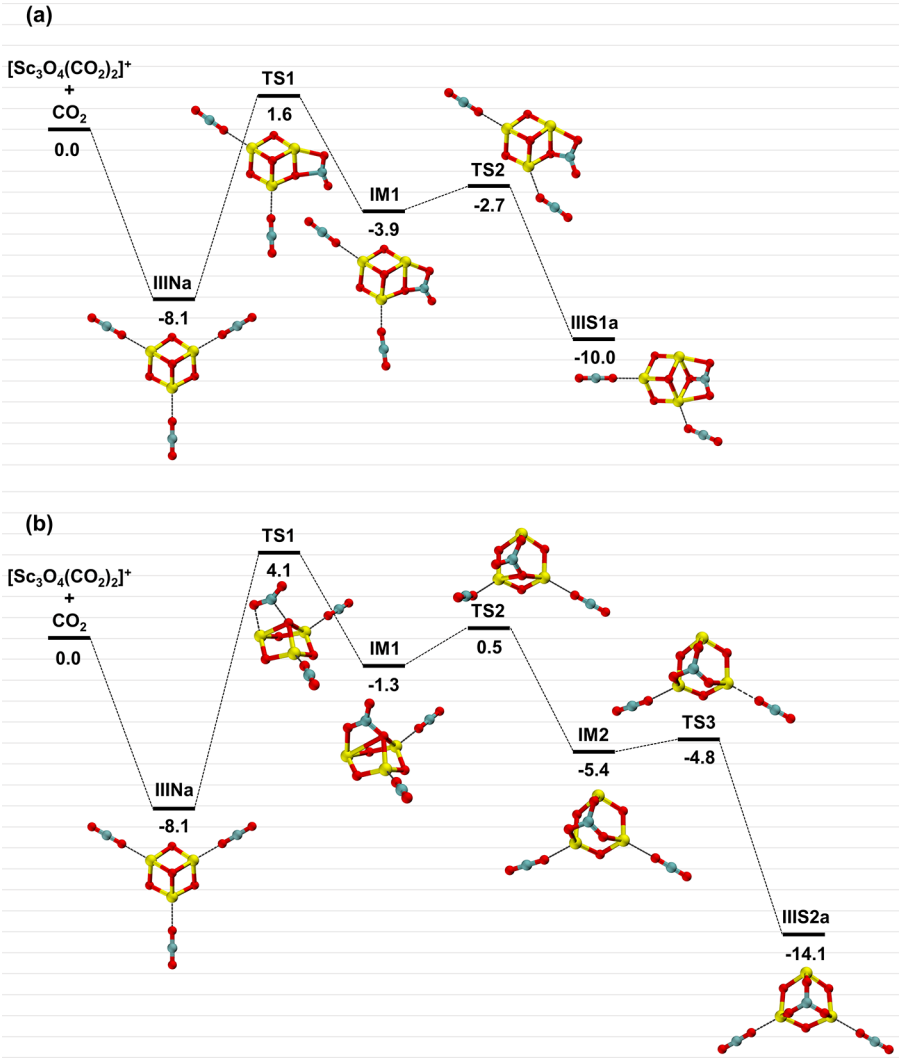

Figure 7. Reaction pathways for the transformation from isomer **IIINa** to **IIIS1a** (a) and **IIIS2a** (b) calculated at the PBE0-D3(BJ)/def2-TZVP level of theory. Relative Gibbs free energies at 298 K are given in kcal mol^{-1}.

Next, the possible contribution of isomers containing a center carbonate core structure was analyzed. The corresponding simulated spectra of isomers **IIIS2a–b** and **IIID2a–d** are provided and compared with the experimental spectrum, as shown in Figure 6. Among the S2 structural motif, isomer **IIIS2a** with C_s symmetry is formed by two CO_2 molecules attached to two Sc atoms of isomer **IS2a** in an end-on configuration. Because of the symmetry of its geometric arrangement, the oscillator in the frequency range of the CO_2 antisymmetric stretching vibration originates from the coupling of two CO_2 molecules. The out-of-phase and in-phase combinations correspond to two IR absorptions at 2381 and 2386 cm^{-1}, which merge into a main band at 2381 cm^{-1} in the simulated IR spectrum. For isomer **IIIS2b**, two CO_2 molecules are bound to the same Sc atom in isomer **IS2a**, with their antisymmetric stretching vibration frequencies predicted to be 2362 and 2379 cm^{-1}, respectively.

In the D2 category, isomers **IIID2a** and **IIID2b** share an identical core structure, as do isomers **IIID2c** and **IIID2d**. The main difference between the two core structures is the relative orientation of the bridge carbonate moiety relative to the center carbonate moiety. The antisymmetric stretching vibrational frequencies of CO_2 molecules in isomers **IIID2a–d** are calculated to be 2385, 2378, 2385, and 2385 cm^{-1}, respectively, with the IR absorption features of three structures notably coinciding at the same position. Overall, isomers with a center carbonate structural motif show a more pronounced blue-shift in their IR signatures compared with isomers featuring only bridge carbonate structures. Therefore, the contribution of the "2" isomers plays a minor role in the experimental spectrum, where the underlying reason might be consistent with the analysis conducted on the $[Sc_3O_4(CO_2)_2]^+$ ion–molecule complex.

Potential energy surfaces describing the conversion processes from low-lying end-on isomer **IIINa** to carbonate structures **IIIS1a** and **IIIS2a** are presented in Figure 7. Both pathways follow similar structural rearrangement patterns as discussed for the transition of the core ion and the n = 2 complex. The energy barrier for the first step in the transformation of isomer **IIINa** to **IIIS2a** is calculated to be 12.2 kcal mol^{-1}, which is 2.5 kcal mol^{-1} higher than that for the transformation to isomer **IIIS1a**. In comparison with the cases examined above, no significant reduction in the differences between the energy barriers for the transformation from end-on isomers to center and bridge carbonate structures has been observed. The distortion energies of $[Sc_3O_4]$ and

https://doi.org/10.1021/acs.jpca.4c04163
J. Phys. Chem. A 2024, 128, 7158–7166

$[CO_2]$ parts that are required to distort their initial geometries into the TS structures are summarized in Table S2, as well as the corresponding instantaneous interaction energies. Upon close examination of the calculated distortion energies, a consistently higher energy cost associated with both $[Sc_3O_4]$ and $[CO_2]$ components is evident for the conversion processes leading to center carbonate structures. Consequently, the greater energy barriers for the formation of center carbonate structures can be attributed to the higher energy expenses for structural distortion.

4. CONCLUSIONS

In this study, we use mass-selected infrared photodissociation spectroscopy coupled with quantum chemical calculations to elucidate the adsorption patterns of CO_2 molecules on the $Sc_3O_4^+$ cation. The theoretical results show that there are weakly bound species along with bridge and center carbonate-containing configurations for the $[Sc_3O_4(CO_2)_n]^+$ (n = 2, 3) ion−molecule complexes. The energetic preference for structures featuring carbonate groups indicates the capability of the $Sc_3O_4^+$ cation in facilitating the carbonation of adsorbed CO_2 molecules. Spectral assignments suggest that isomers with a bridge carbonate core structure are predominantly present in the experiment, as supported by the comparison with simulated infrared spectra of different low-lying complexes. Potential energy profiles reveal lower energy barriers and a simpler reaction pathway for the formation of a bridge carbonate moiety via the reaction of an end-on coordinated CO_2 molecule with the $Sc_3O_4^+$ cation, presenting plausible interpretations for the experimental observations. Our findings provide valuable insights into the mechanisms involved in the adsorption and carbonation of CO_2 molecules on scandium oxide cations.

■ ASSOCIATED CONTENT

Supporting Information

The Supporting Information is available free of charge at https://pubs.acs.org/doi/10.1021/acs.jpca.4c04163.

Binding energies of CO_2 ligands and the corresponding number of dissociating photons for isomers of the $[Sc_3O_4(CO_2)_2]^+$ ion−molecule complex at the PBE0-D3(BJ)/def2-TZVP level of theory (Table S1); distortion energies of $[Sc_3O_4]$ and $[CO_2]$ parts and their interaction energies calculated for all transition state structures corresponding to the first transition steps from end-on isomers (**INa**−**IIINa**) to different carbonate structures at the PBE0-D3(BJ)/def2-TZVP level of theory (Table S2); typical time-of-flight (TOF) mass spectrum produced by pulsed laser vaporization of a scandium metal target in expansion of helium seeded with carbon dioxide (Figure S1); and reaction pathways for the transformation from isomer **IINa** to **IIS2a** calculated at the PBE0-D3(BJ)/def2-TZVP level of theory (Figure S2) (PDF)

■ AUTHOR INFORMATION

Corresponding Author

Jia Han − *Hefei National Research Center for Physical Sciences at the Microscale, University of Science and Technology of China, Hefei 230026, China;* orcid.org/0009-0004-0578-6716; Email: jiahan@ustc.edu.cn

Authors

Pengcheng Liu − *Anhui Institute of Optics and Fine Mechanics, Hefei Institutes of Physical Science, Chinese Academy of Sciences, Hefei 230031, China; Science Island Branch, Graduate School, University of Science and Technology of China, Hefei 230026, China*

Haili Yu − *Department of Chemical Physics, University of Science and Technology of China, Hefei 230026, China*

Yan Chen − *Department of Chemical Physics, University of Science and Technology of China, Hefei 230026, China*

Xiaoguo Zhou − *Hefei National Research Center for Physical Sciences at the Microscale and Department of Chemical Physics, University of Science and Technology of China, Hefei 230026, China;* orcid.org/0000-0002-0264-0146

Complete contact information is available at: https://pubs.acs.org/10.1021/acs.jpca.4c04163

Notes

The authors declare no competing financial interest.

■ ACKNOWLEDGMENTS

This work was financially supported by the National Natural Science Foundation of China (nos. 22073088 and 91544228). All DFT calculations were performed on the supercomputing system in the Supercomputing Center of the University of Science and Technology of China.

■ REFERENCES

(1) Tappe, N. A.; Reich, R. M.; D'Elia, V.; Kühn, F. E. Current Advances in the Catalytic Conversion of Carbon Dioxide by Molecular Catalysts: An Update. *Dalton Trans.* **2018**, *47*, 13281−13313.

(2) Hepburn, C.; Adlen, E.; Beddington, J.; Carter, E. A.; Fuss, S.; Mac Dowell, N.; Minx, J. C.; Smith, P.; Williams, C. K. The Technological and Economic Prospects for CO_2 Utilization and Removal. *Nature* **2019**, *575*, 87−97.

(3) Dodson, L. G.; Thompson, M. C.; Weber, J. M. Characterization of Intermediate Oxidation States in CO_2 Activation. *Annu. Rev. Phys. Chem.* **2018**, *69*, 231−252.

(4) Taifan, W.; Boily, J.-F.; Baltrusaitis, J. Surface Chemistry of Carbon Dioxide Revisited. *Surf. Sci. Rep.* **2016**, *71*, 595−671.

(5) Chen, H.; Nanayakkara, C. E.; Grassian, V. H. Titanium Dioxide Photocatalysis in Atmospheric Chemistry. *Chem. Rev.* **2012**, *112*, 5919−5948.

(6) Tyagi, P.; Singh, D.; Malik, N.; Kumar, S.; Singh Malik, R. Metal Catalyst for CO_2 Capture and Conversion into Cyclic Carbonate: Progress and Challenges. *Mater. Today* **2023**, *65*, 133−165.

(7) Baltrusaitis, J.; Schuttlefield, J.; Zeitler, E.; Grassian, V. H. Carbon Dioxide Adsorption on Oxide Nanoparticle Surfaces. *Chem. Eng. J.* **2011**, *170*, 471−481.

(8) Busca, G.; Lorenzelli, V. Infrared Spectroscopic Identification of Species Arising From Reactive Adsorption of Carbon Oxides on Metal Oxide Surfaces. *Mater. Chem.* **1982**, *7*, 89−126.

(9) Hakim, A.; Marliza, T. S.; Abu Tahari, N. M.; Wan Isahak, R. W. N.; Yusop, R. M.; Mohamed Hisham, W. M.; Yarmo, A. M. Studies on CO_2 Adsorption and Desorption Properties from Various Types of Iron Oxides (FeO, Fe_2O_3, and Fe_3O_4). *Ind. Eng. Chem. Res.* **2016**, *55*, 7888−7897.

(10) Song, G.; Zhu, X.; Chen, R.; Liao, Q.; Ding, Y.-D.; Chen, L. An Investigation of CO_2 Adsorption Kinetics on Porous Magnesium Oxide. *Chem. Eng. J.* **2016**, *283*, 175−183.

(11) Hübner, O.; Himmel, H.-J. Metal Cluster Models for Heterogeneous Catalysis: A Matrix-Isolation Perspective. *Chem. − Eur. J.* **2018**, *24*, 8941−8961.

(12) Zhou, M.; Zhou, Z.; Zhuang, J.; Li, Z. H.; Fan, K.; Zhao, Y.; Zheng, X. Carbon Dioxide Coordination and Activation by Niobium Oxide Molecules. *J. Phys. Chem. A* **2011**, *115*, 14361−14369.
(13) Zhuang, J.; Li, Z. H.; Fan, K.; Zhou, M. Matrix Isolation Spectroscopic and Theoretical Study of Carbon Dioxide Activation by Titanium Oxide Molecules. *J. Phys. Chem. A* **2012**, *116*, 3388−3395.
(14) Zhang, Q.; Qu, H.; Chen, M.; Zhou, M. Carbon Dioxide Activation by Scandium Atoms and Scandium Monoxide Molecules: Formation and Spectroscopic Characterization of $ScCO_3$ and $OCScCO_3$ in Solid Neon. *J. Phys. Chem. A* **2016**, *120*, 425−432.
(15) Koyanagi, G. K.; Bohme, D. K. Gas-Phase Reactions of Carbon Dioxide with Atomic Transition-Metal and Main-Group Cations: Room-Temperature Kinetics and Periodicities in Reactivity. *J. Phys. Chem. A* **2006**, *110*, 1232−1241.
(16) Sievers, M. R.; Armentrout, P. B. Gas Phase Activation of Carbon Dioxide by Niobium and Niobium Monoxide Cations. *Int. J. Mass Spectrom.* **1998**, *179*−*180*, 103−115.
(17) Zhao, Z.; Kong, X.; Yuan, Q.; Xie, H.; Yang, D.; Zhao, J.; Fan, H.; Jiang, L. Coordination-Induced CO_2 Fixation into Carbonate by Metal Oxides. *Phys. Chem. Chem. Phys.* **2018**, *20*, 19314−19320.
(18) Brewer, E. I.; Green, A. E.; Gentleman, A. S.; Beardsmore, P. W.; Pearcy, P. A. J.; Meizyte, G.; Pickering, J.; Mackenzie, S. R. An Infrared Study of CO_2 Activation by Holmium Ions, Ho^+ and HoO^+. *Phys. Chem. Chem. Phys.* **2022**, *24*, 22716−22723.
(19) Liu, P.; Han, J.; Chen, Y.; Lu, S.; Su, Q.; Zhou, X.; Zhang, W. Carbon Dioxide Activation by Discandium Dioxide Cations in the Gas Phase: A Combined Investigation of Infrared Photodissociation Spectroscopy and DFT Calculations. *Phys. Chem. Chem. Phys.* **2023**, *25*, 32853−32862.
(20) Yang, D.; Su, M.-Z.; Zheng, H.-J.; Zhao, Z.; Kong, X.-T.; Li, G.; Xie, H.; Zhang, W.-Q.; Fan, H.-J.; Jiang, L. Infrared Spectroscopy of CO_2 Transformation by Group III Metal Monoxide Cations. *Chin. J. Chem. Phys.* **2020**, *33*, 160−166.
(21) Han, J.; Yang, Y.; Qiu, B.; Liu, P.; Wu, X.; Wang, G.; Liu, S.; Zhou, X. Infrared Photodissociation Spectroscopy of Mass-Selected $[TaO_3(CO_2)_n]^+$ (n = 2−5) Complexes in the Gas Phase. *Phys. Chem. Chem. Phys.* **2023**, *25*, 13198−13208.
(22) Walker, N. R.; Grieves, G. A.; Walters, R. S.; Duncan, M. A. The Metal Coordination in $Ni^+(CO_2)$n and $NiO_2^+(CO_2)_m$ Complexes. *Chem. Phys. Lett.* **2003**, *380*, 230−236.
(23) Iskra, A.; Gentleman, A. S.; Cunningham, E. M.; Mackenzie, S. R. Carbon Dioxide Binding to Metal Oxides: Infrared Spectroscopy of $NbO_2^+(CO_2)_n$ and $TaO_2^+(CO_2)_n$ Complexes. *Int. J. Mass Spectrom.* **2019**, *435*, 93−100.
(24) Kong, X.; Shi, R.; Wang, C.; Zheng, H.; Wang, T.; Liang, X.; Yang, J.; Jing, Q.; Liu, Y.; Han, H.; et al. Interaction between CO_2 and NbO_2^+: Infrared Photodissociation Spectroscopic and Theoretical Study. *Chem. Phys.* **2020**, *534*, No. 110755.
(25) Lu, T.; Chen, F. Multiwfn: A Multifunctional Wavefunction Analyzer. *J. Comput. Chem.* **2012**, *33*, 580−592.
(26) Lu, T. *Molclus* Program, 1.9.9.3; http://www.keinsci.com/research/molclus.html, 2021.
(27) Bannwarth, C.; Ehlert, S.; Grimme, S. GFN2-xTB—An Accurate and Broadly Parametrized Self-Consistent Tight-Binding Quantum Chemical Method with Multipole Electrostatics and Density-Dependent Dispersion Contributions. *J. Chem. Theory Comput.* **2019**, *15*, 1652−1671.
(28) Grimme, S.; Bannwarth, C.; Shushkov, P. A Robust and Accurate Tight-Binding Quantum Chemical Method for Structures, Vibrational Frequencies, and Noncovalent Interactions of Large Molecular Systems Parametrized for All spd-Block Elements (Z = 1−86). *J. Chem. Theory Comput.* **2017**, *13*, 1989−2009.
(29) Adamo, C.; Barone, V. Toward Reliable Density Functional Methods without Adjustable Parameters: The PBE0Model. *J. Chem. Phys.* **1999**, *110*, 6158−6170.
(30) Grimme, S.; Ehrlich, S.; Goerigk, L. Effect of the Damping Function in Dispersion Corrected Density Functional Theory. *J. Comput. Chem.* **2011**, *32*, 1456−1465.
(31) Fukui, K. Formulation of the Reaction Coordinate. *J. Phys. Chem.* **1970**, *74*, 4161−4163.
(32) Fukui, K. The Path of Chemical Reactions-the IRC Approach. *Acc. Chem. Res.* **1981**, *14*, 363−368.
(33) Gonzalez, C.; Schlegel, H. B. Reaction Path Following in Mass-Weighted Internal Coordinates. *J. Phys. Chem.* **1990**, *94*, 5523−5527.
(34) Truhlar, D. G.; Gordon, M. S. From Force Fields to Dynamics: Classical and Quantal Paths. *Science* **1990**, *249*, 491−498.
(35) Frisch, M. J.; Trucks, G. W.; Schlegel, H. B.; Scuseria, G. E.; Robb, M. A.; Cheeseman, J. R.; Scalmani, G.; Barone, V.; Petersson, G. A.; Nakatsuji, H.,et al.*Gaussian 16* Rev. C.01, Gaussian Inc.: Wallingford, CT, 2016.
(36) Liu, P.; Han, J.; Chen, Y.; Yu, H.; Zhou, X.; Zhang, W. Binding Strengths and Orientations in CO_2 Adsorption on Cationic Scandium Oxides: Governing Factor Revealed by a Combined Infrared Spectroscopy and Theoretical Study. *J. Phys. Chem. A* **2024**, *128*, 3007−3014.
(37) Debnath, S.; Song, X.; Fagiani, M. R.; Weichman, M. L.; Gao, M.; Maeda, S.; Taketsugu, T.; Schöllkopf, W.; Lyalin, A.; Neumark, D. M.; et al. CO_2 Adsorption on $Ti_3O_6^-$: A Novel Carbonate Binding Motif. *J. Phys. Chem. C* **2019**, *123*, 8439−8446.
(38) Debnath, S.; Song, X.; Fagiani, M. R.; Weichman, M. L.; Gao, M.; Maeda, S.; Taketsugu, T.; Schöllkopf, W.; Lyalin, A.; Neumark, D. M.; et al. Correction to "CO_2 Adsorption on $Ti_3O_6^-$: A Novel Carbonate Binding Motif. *J. Phys. Chem. C* **2020**, *124*, 6952−6953.

https://doi.org/10.1021/acs.jpca.4c04163
J. Phys. Chem. A 2024, 128, 7158−7166